Manufacturing Rev. **11**, 14 (2024)

https://doi.org/10.1051/mfreview/2024012

Manufacturing Review
Available online at:
https://mfr.edp-open.org

RESEARCH ARTICLE OPEN ACCESS

Prediction models and multi-objective optimization of the single deposited tracks in laser direct metal deposition of 316L stainless steel

Khoa Doan Tat[1], Van Thao Le[2,*], and Nguy Duong Van[1]

[1] Faculty of Mechanical Engineering, Le Quy Don Technical University, Hanoi, Vietnam
[2] Advanced Technology Center, Le Quy Don Technical University, Hanoi, Vietnam

Received: 9 January 2024 / Accepted: 6 May 2024

Abstract. Laser direct metal deposition (LDMD) is a metal additive manufacturing process, which uses a laser source to melt metal powder and deposit the molten metal into the part layer-by-layer through a nozzle. With suitable process parameters and setting conditions, a component can be fabricated with a full density. In this process, the shape of single tracks is a key indicator, which directly prescribes the quality of the process and the fabricated component. To fabricate a complex component, especially that with thin-wall structures with free of defects, controlling the single tracks' geometry and the understanding on the effects of the process parameters are essential. Therefore, this article focuses on studying the effects of process variables on single tracks' attributes in the LDMD process of SS316L and identifying the optimum variables for the deposition of SS316L thin wall structures. The observed results indicated that, among the process parameters (the scanning speed V_s, the laser power P_l, and the powder feed rate f_p), P_l exhibits the highest impact contribution to the models of the deposited track width w and the deposited track penetration p with a contribution of 71.83% and 87.68%, respectively. V_s exhibits the highest contribution to the models of the deposited track height h a contribution of 49.86%. On the other hand, f_p shows an insignificant impact contribution to the w and p models. All the developed models feature a high prediction accuracy with the values of determination coefficients R^2 of 97.89%, 97.08%, 99.11% for w, h, and p, respectively, indicating that they can be used to prediction w, h, and p with high confidence and precision levels. Moreover, the optimization results achieved by different methods (i.e., GRA, TOPSIS, and PSO+TOPSIS) demonstrated that the PSO and TOPSIS combination can be used to find out the most optimal process parameters (i.e., $V_s = 6$ mm/s, $P_l = 263.63$ W, and $f_p = 18$ g/min) to build thin-walled structures in SS316L by LDMD.

Keywords: Laser direct metal deposition / 316L / optimization / GRA / TOPSIS / PSO

1 Introduction

Laser direct metal deposition (LDMD) is a metal additive manufacturing (AM) technology that sprays metal powder with a laser source coaxially via a nozzle to melt powder and directly deposit into the workpiece layer-by-layer [1–3]. The thickness of layers normally ranges from 0.1 mm to 2 mm. Based on the layer deposition principle, LDMD can build near-net shape and complex parts without the need of cutting tools and other additional resources as in traditional manufacturing processes (e.g., machining) [4,5]. Nowadays, LDMD is a promising AM technology applied in many fields, for example aeronautics, automobile, molds and dies, repairing of parts, and rapid manufacturing of spare parts [6,7].

In LDMD processes, to create a robust and tightly bonded thick clad layer on the substrate, it is essential to meticulously manage the geometric attributes of an individual deposited track [8–13]. Furthermore, optimizing the processing parameters is important, especially concerning the percentage of porosity and the geometric qualities, to guarantee superior clad performance during the deposition [9–11,14–17]. There are several process parameters that directly influence the quality of single tracks, for example, the laser power P_l (W), the powder feeding rate f_p (g/min), the scanning speed of the nozzle V_s (mm/s), the size of the laser beam spot, the amount of carrying and shielding gas, the powder size, and so on. However, the key process variables identified by previous

* e-mail: vtle@lqdtu.edu.vn

studies are the laser power P_l (W), the powder feeding rate f_p (g/min), the scanning speed of the nozzle V_s (mm/s) [14,18,19].

Numerous studies have been conducted to explore how the key parameters influence both the geometry of single deposited tracks and the deposited materials' integrity. For example, Errico et al. [20] examined the impact of parameters, including P_l, f_p, V_s and the carrying gas flow rate on microstructures and porosity of SS 304 deposited by LDMD. Ascari et al. [21] conducted an extensive series of analysis to study how process parameters influence geometries, surface roughness, microstructures, tensile strengths, hardness, and productivity in the deposition of bulk materials of SS 316L. Campanelli et al. [22] investigated the effects of P_l, f_p, V_s, and the overlapping distance between successive tracks in assessing the properties of deposited 18 Ni 300 maraging steel. To develop analytical models, which present the relationship between geometry attributes of single deposited tracks (e.g., width, height, penetration, and contact angle) and the process parameters P_l, f_p, and V_s, several authors have adopted the linear model $Y = a * X + b$ with $X = P_l^{\alpha} * V_s^{\beta} * f_p^{\gamma}$ [14,18,19]. The coefficients of the models were determined based on the experimental data with the help of Excel and Matlab software. However, the method to estimate (α, β, and γ) was not detailed in these studies. Most of these works adopted the "*trial and error*" method so that the determination coefficient of the models (R^2) reach a maximum value possible [18].

Concerning the Optimization of the single deposited tracks in the LDMD process, Vaughan et al. [23] proposed a framework for optimizing single tracks considering the laser power, the scanning speed, and the powder feed rate, to obtain a dense bulk components of high strength steels. Zardoshtian et al. [23] adopted the response surface methodology (RSM) to optimize the single-track geometry of CuCrZr alloy deposited by LDMD. They stated that the estimated optimal parameter, including the scanning speed of 4.5 mm/s, the laser power of 1550 W, and the powder feed rate of 12 g/min enabled producing single track geometries with a good shape, sufficient dilution, and at the maximum rate of deposition. Recently, Javidrad et al. [11] performed a study on the optimization of the process parameter for the LDED process of Inconel 738LC. The authors aimed at minimizing the porosity, while maximizing the production rate and using the RSM method to resolve such a multi-objective optimization problem. Pandey et al. [24] also used the RSM method to optimize the single tracks' geometries when depositing 15Cr5Ni stainless steel. Meanwhile, Du et al. [23] employed the combination of TOPSIS (Technique for Order Preference by Similarity to Ideal Solution) and GRA (Grey-Relational Analysis) for optimizing single tracks in laser cladding of 15-5PH steel.

To the best of the authors' knowledge, until now, very few authors have paid attention to the prediction and multi-objective optimization of the single deposited tracks in LDMD processes. To fill this knowledge gap, this paper aims to develop the prediction models for geometrical attributes of single tracks in LDMD of SS 316L. The models are developed by using experimental data. After that, several multi-objective optimization methods, including GRA, TOPSIS, and PSO (Particle Swarm Optimization) algorithm combined with TOPSIS are considered to identify the optimal process parameters that enable to obtain the expected attributes of single tracks for specific applications. GRA and TOPSIS methods are widely used in different fields to determine the optimal solution among a set of available alternatives [25,26]. On the other hand, PSO is a nature-inspired optimization technique used to find all the feasible optimal solutions in the search space [27].

2 Materials and methods

2.1 Materials and equipment

The DLMD system used in this study is comprised of a 0.5 kW fiber laser, a powder feeder system, a deposition nozzle, and a three-axis CNC mechanism (Fig. 1a). The SS 316L powder was utilized in the experiment. The particle size ranges from 15 to 55 μm with the average size of 25.56 μm and the standard deviation of 9.22 μm (Figs. 1b and 1c) and the chemical composition is given in Tab. 1. SS 316L plates with dimensions of 200 × 100 × 10 mm and its composition indicated in Table 2 were utilized as the substrate. Before the deposition, the metal powder was dried in a vacuum drying oven at 200 °C for 4 h to eliminate moisture. The substrate was polished with sandpaper and then cleaned with acetone and ethanol to remove grease and stains.

2.2 Fabrication of samples and data collection

In the LDMD process, there are many process parameters that could influence the geometry and quality of tracks, such as the laser beam spot diameter, the pressure and flowrate of carrying/shielding gas, the particle size distribution, the laser power P_l, the powder feeding rate f_p, the scanning speed of the nozzle V_s, and so on [8,9,11,17,28–31]. However, the laser power, the powder feeding rate, and the scanning speed are identified as the key parameters that most considerably impact on the temperature distribution, the melting pool dimensions, and the geometry of tracks [13,16]. Moreover, in the experiment, the change of these parameters is simpler and more practical than other ones, such as the laser beam spot diameter and the particle size distribution. Therefore, in this research, we consider the scanning speed V_s, the laser powder P_l, and the powder feeding rate f_p for the parametric investigation and optimization, while other parameters were fixed at a constant value. To fabricate the single deposited tracks, the experimental plan was designed according to L9 orthogonal array Taguchi method with three levels for each parameter, as shown in Table 2. As a result, there are nine experimental runs. The nice single tracks were deposited and cleaned, as shown in Figure 2a. All the depositions were performed in a building chamber filled with a shielding gas of argon, where the oxygen level is less than 20 ppm. The rate of shielding and carrying gas was maintained at 6 L/min. The distance from the laser head tip to the substrate's surface was fixed at 15 mm, and the laser beam spot diameter is controlled at 1 mm.

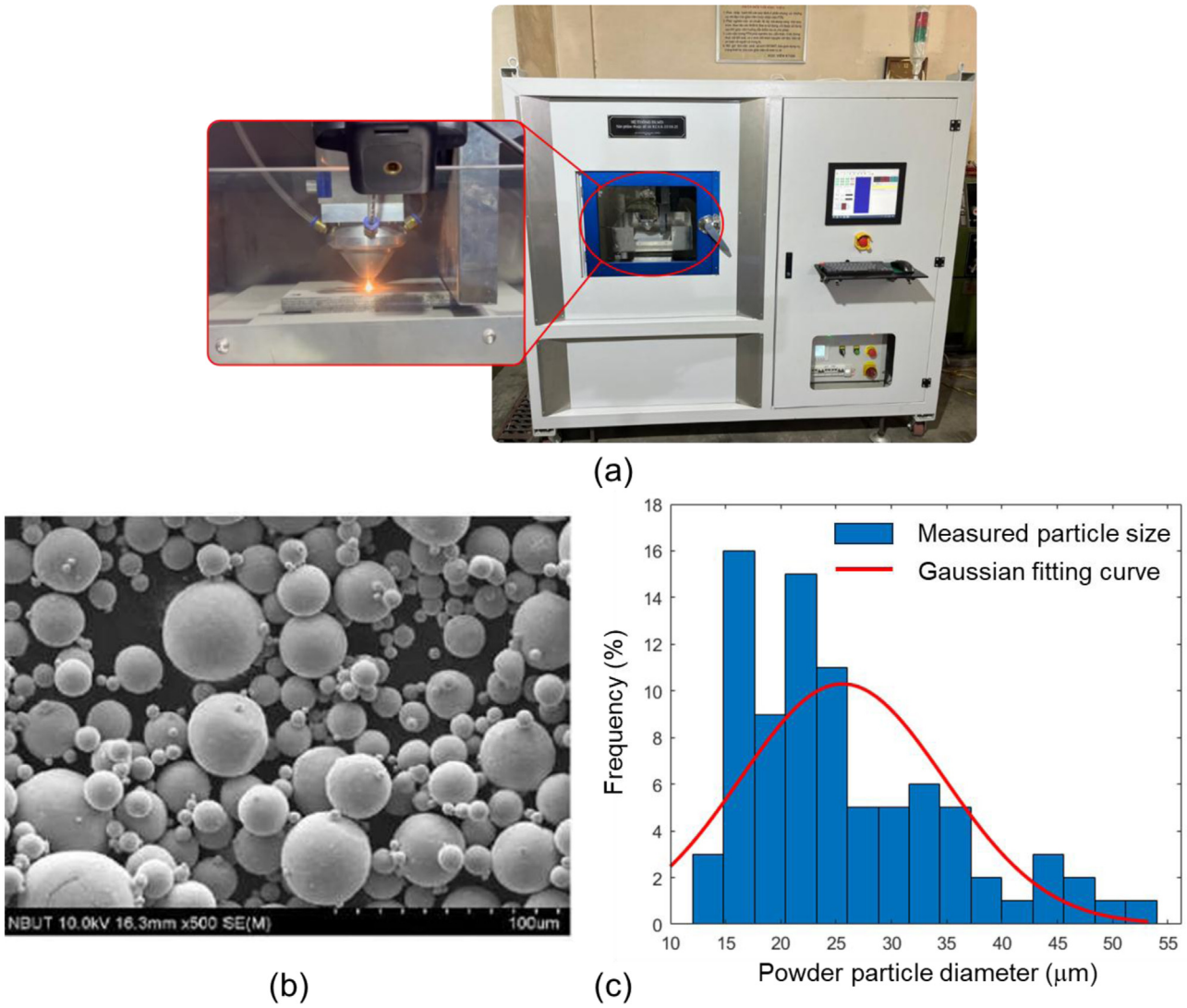

Fig. 1. (a) The LDMD system, (b) a SEM image of SS 316L powder, and (c) the powder size distribution.

Table 1. Chemical composition of powder and substrate material (wt.%).

Element	C	Si	Mn	P	S	Cr	Ni	Mo	Fe
316L SS powder	0.02	0.0	1.06	0.005	0.003	17	12	2.04	Bal.
316L SS Substrate	0.03	0.75	2.0	0.045	0.03	16–18	10–14	2–3	Bal.

Table 2. Studied variables and their levels.

Variables	Levels		
	1	2	3
V_s (mm/s)	6	8	10
P_l (W)	200	250	300
f_p (g/min)	6	12	18

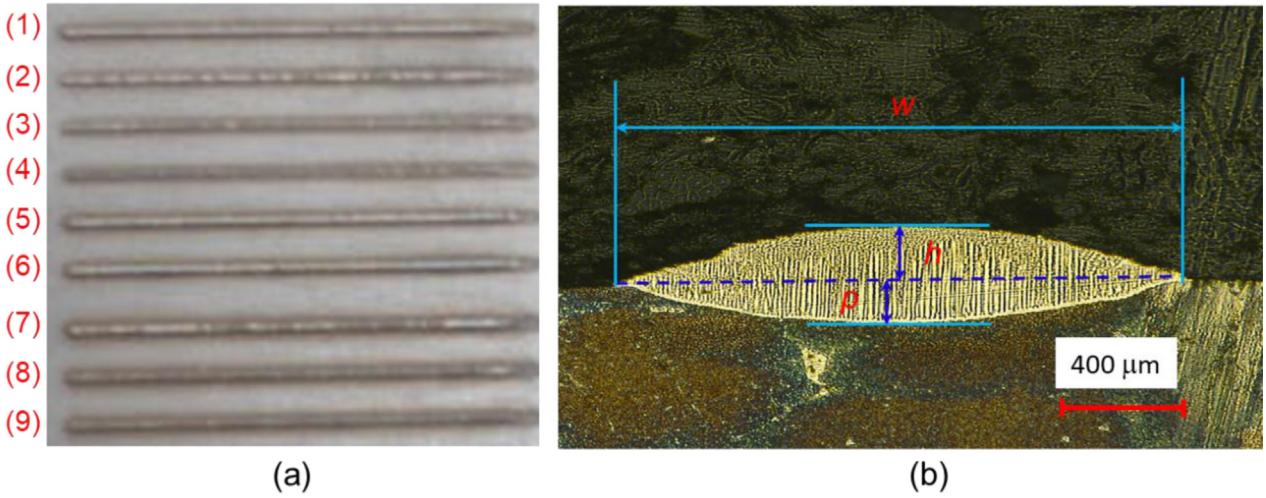

Fig. 2. (a) Deposited single tracks and (b) a cross-section of the deposited single track (6).

Table 3. Experimental runs and the collected data.

No.	V_s (mm/s)	P_l (W)	f_p (g/min)	w (mm)	h (mm)	p (mm)
1	6	200	6	1.55	0.12	0.07
2	6	250	12	1.63	0.18	0.09
3	6	300	18	1.75	0.24	0.12
4	8	200	12	1.51	0.10	0.06
5	8	250	18	1.56	0.14	0.08
6	8	300	6	1.70	0.14	0.12
7	10	200	18	1.39	0.09	0.04
8	10	250	6	1.55	0.06	0.09
9	10	300	12	1.64	0.13	0.11

It can be found that, on the top view (Fig. 2a), all the tracks were regular and stable. As a result, we can suppose that all these single tracks have almost constant value of track width and track height, especially in the middle region of each track. Therefore, we decided to analyze the tracks' attributes (including the width w, height h, and penetration depth p) from the middle of their length. This approach enables avoiding the impact of edge effects, and it is also widely used by previous studies in the literature [15,16,32]. Whereby, the cross-sections of each single track in the middle regions were extracted, ground, polished and chemically etched to measure the attributes (w, h, and p). The measurement of w, h, and p were performed with the help of an optical microscope (AXIO A2M, Carl Zeiss). The experimental matrix and measured data were presented in Table 3.

The measured data was used to analyze the influence of process variables on the attributes of single deposited tracks and to develop the prediction models. The development of prediction models and the analysis of variance are performed with the aid of Minitab 19 software.

2.3 Optimization methods

In this study, we aim to find out the optimal process parameters for the building of thin-wall structures by the LDMD process. In this case, the width and the penetration of single deposited tracks are preferred to be minimized, while the height of the single deposited track is desired to be maximized. As a result, the multi-objective optimization issue is described as: "Find (V_s, P, and f_p) to minimize (w and p) while maximize h, subject to $8 \leq V_s\,(\text{mm/s}) \leq 10$, $230 \leq P\ (W) \leq 270$, and $8 \leq f_p\ (\text{g/min}) \leq 12$".

To resolve such a problem, different methods are employed and evaluated to select the best one. As mentioned earlier, the three following methods are examined, including PSO combined with TOPSIS, GRA, and TOPSIS. These methods are briefly described, as follows.

2.3.1 GRA

GRA is one of the methods widely used for the multi-objective optimization in manufacturing processes [33]. This method consists of transforming a multi-objective

issue to a mono-objective one. The GRA procedure is composed of the following steps:

(1) Normalizing the kth objective using the following criteria:

$$r_i^{(n)}(k) = \frac{\underbrace{\max}_{i}\left(r_i^{(0)}(k)\right) - r_i^{(0)}(k)}{\underbrace{\max}_{i}\left(r_i^{(0)}(k)\right) - \underbrace{min}_{i}\left(r_i^{(0)}(k)\right)} \quad (1)$$

if the objective respects the smallest-the-best criterion.

$$r_i^{(n)}(k) = \frac{r_i^{(0)}(k) - \underbrace{min}_{i}\left(r_i^{(0)}(k)\right)}{\underbrace{\max}_{i}\left(r_i^{(0)}(k)\right) - \underbrace{min}_{i}\left(r_i^{(0)}(k)\right)} \quad (2)$$

if the objective respects the biggest-the-best criterion.

where $r_i^{(0)}(k)$ is the value of the kth objective measured at the ith trial, $\underbrace{\max}_{i}\left(r_i^{(0)}(k)\right)$ and $\underbrace{min}_{i}\left(r_i^{(0)}(k)\right)$ are the highest and the smallest values of the kth objective measured in the experiment, and $r_i^{(n)}(k)$ is the normalized value of the kth attribute measured at the ith trial. In this study, the objectives (w and p) are normalized according to equation (1) and h is normalized according to equation (2).

(2) Calculating GRCs (grey-relational coefficients) for the normalized data using equation (3):

$$\mathrm{GRC}_i = \frac{\theta_{min} + \varphi{*}\theta_{\max}}{\theta_{oi}(k) - \theta_{min}}, \quad (3)$$

where $0 \le \mathrm{GRC}_i \le 1, \theta_{oi}(k), \theta_{min}$, and θ_{max} are calculated as equations (4), (5), and (6):

$$\theta_{oi}(k) = \left|r_0^{(n)}(k) - r_i^{(n)}(k)\right|, \quad (4)$$

$$\theta_{min} = \underbrace{min}_{\forall i}\ \underbrace{min}_{\forall k}\left(\left|r_0^{(n)}(k) - r_i^{(n)}(k)\right|\right), \quad (5)$$

$$\theta_{\max} = \underbrace{\max}_{\forall i}\ \underbrace{\max}_{\forall k}\left(\left|r_0^{(n)}(k) - r_i^{(n)}(k)\right|\right), \quad (6)$$

$r_0^{(n)}(k)$ is the reference sequence, for example, $r_0^{(n)}(k) = \underbrace{\max}_{i}\left(r_i^{(n)}(k)\right)$, and φ is a coefficient in the range of (0, 1). In this study, $\varphi = 0.5$.

(3) Calculating the GRGs (grey-relational grades) by equation (7):

$$\mathrm{GRG}_j = \sum \omega_j * GRC_j, \quad (7)$$

where ω_j is the weight of the jth objective with $\sum\omega_j = 1$ and $0 < \mathrm{GRG}_j\ 1$.

Finally, the optimized solution is corresponding to the maximum value of GRG_j.

2.3.2 TOPSIS

As mentioned earlier, TOSIS relies on the concept that the optimal alternative is the nearest to the best solution and it is the farthest from the worst solution [34,35]. The main steps of TOPSIS method are expressed, as follows:

(1) Formulating the decision matrix $\{r_{ij}\}_{\mathrm{nxm}}$, where m is the objective number, n is the trial number in the experiment, and r_{ij} is the value of the jth objective at the ith trial.

(2) Normalizing the decision matrix by equation (8):

$$r'_{ij} = \frac{r_{ij}}{\sqrt{\sum r_{ij}^2}}, \quad (8)$$

(3) Assigning the normalized matrix with the weight of each objective using equation (9):

$$p_{ij} = \omega_j * r'_{ij}, \quad (9)$$

(4) Determining the best solutions (BS) and the worst solutions (WS) using equations (10) and (11):

$$BS = \left\{\underbrace{\max}_{i}(p_{ij}), \underbrace{min}_{i}(p_{ij})\right\} = \{BS_1, BS_2, ..., BS_m\}, \quad (10)$$

$$WS = \left\{\underbrace{min}_{i}(p_{ij}), \underbrace{\max}_{i}(p_{ij})\right\} = \{WS_1, WS_2, ...WS_m\}, \quad (11)$$

(5) Calculating the distance from the BSs and WSs to the feasible solutions using equations (12) and (13), respectively:

$$D_{BS_i} = \sqrt{\sum_{i=1}^{m}(p_{ij} - BS_j)^2}, \quad (12)$$

$$D_{WS_i} = \sqrt{\sum_{i=1}^{m}(p_{ij} - WS_j)^2}, \quad (13)$$

(6) Computing the closest index of the BSs using equation (14):

$$C_{Index}^{i} = \frac{D_{WS_i}}{D_{WS_i} + D_{BS_i}}. \quad (14)$$

The values of C_{Index}^{i} are also in the range of (0, 1), and the optimum solution corresponds to the maximum value of C_{Index}^{i}.

In this study, it is remarked that the weight ω_j for the jth objective in the TOPSIS and GRA is similar and calculated by the CRITIC method [36]. This approach integrates both the inherent conflict aspect and the level of contrast in determining the weight proportion of each response. The steps and equations associated with this approach are following:

(i) Normalizing the decision matrix $\{r_{ij}\}_{\text{nxm}}$ using equation (15):

$$r_{ij} = \frac{r_{ij} - r_j^{worst}}{r_j^{best} - r_j^{worst}}, \tag{15}$$

where r_{ij} is the normalized value of the ith alternative for jth objective, r_j^{worst} and r_j^{worst} are the worst and the best values of the jth objective.

(ii) Calculating the standard deviation of each normalized attribute according to equation (16):

$$\sigma_j = \sqrt{\frac{\sum_{i=1}^{n}(r_{ij} - \overline{r}_j)^2}{n}}, \tag{16}$$

where r_j is the average value of the jth normalized objective.

(iii) Constructing the matrix $[C_{ij}]_{nxn}$ with the linear correlation coefficients C_{ij} between the objectives. C_{ij} is computed according to equation (17):

$$C_{ij} = \frac{\sum_{l=1}^{n}(r_{li} - \overline{r}_i)(r_{lj} - \overline{r}_j)}{\sqrt{\sum_{l=1}^{n}(r_{li} - \overline{r}_i)^2 \sum_{l=1}^{k}(r_{lj} - \overline{r}_j)^2}}, \tag{17}$$

(iv) Calculating the objective information OI_j by equation (18):

$$OI_j = \sigma_j \sum_{l-1}^{n}(1 - C_{ji}), \tag{18}$$

(v) Identifying the weight ω_j or each objective using equation (19):

$$\omega_j = \frac{OI_j}{\sum_{j-1}^{m} OI_j}. \tag{19}$$

2.3.3 PSO algorithm

PSO is an optimization algorithm that mimics the collective behavior observed in flocks of birds or schools of fishes. This algorithm involves the initial creation of a population of particles, including their positions ($\boldsymbol{Posi_i}$) and velocities ($\boldsymbol{Velo_i}$) are randomly assigned within allowable ranges. Each particle, specifically its position, represents a potential solution to the problem [28]. In essence, each position can be considered as a vector: $\boldsymbol{Posi_i} = (Posi_{i,1}, Posi_{i,2}, ..., Posi_{i,N})$, where '$i$' signifies the particle index, and 'N' denotes the number of design variables, and the particle has a velocity: $\boldsymbol{Velo_i} = (Velo_{i,1}, Velo_{i,2}, ..., Velo_{i,N})$. The position of each particle can be seen as a unique point within the solution space. The objective function is used to evaluate each position's performance. During each iteration, the best position for each particle ($\boldsymbol{Posi_{ibest}}$) and the best position among all particles ($\boldsymbol{Global_{best}}$) are updated and saved when necessary. Additionally, in each iteration, all the elements of the velocity and position vectors for all particles are updated using equations (20) and (21), respectively:

$$\begin{aligned} Velo_{i,j}^{new} = {} & Velo_{i,j}^{old} * \omega + C_1 * R_1 \\ & * \left(Posi_{ibest,j} - Posi_{i,j}\right) + C_2 * R_2 \\ & * \left(Global_{best,j} - Posi_{i,j}\right), \end{aligned} \tag{20}$$

$$Posi_{i,j}^{new} = Posi_{i,j}^{old} + Velo_{i,j}^{new}, \tag{21}$$

where i and j present the particle's index and the dimension of each design parameter, respectively. ωs the inertial weight. C_1 and C_2 are the coefficients of acceleration. R_1 and R_2 are the random numbers induced through a uniform distribution. When the termination criteria are satisfied, the optimum solution is the last best position of all the particles (i.e., the last $\boldsymbol{Global_{best}}$). The procedure of the PSO algorithm is drawn in Figure 3.

3 Results and discussion

3.1 Development of prediction models

In this study, all the prediction models of single-track attributes (i.e., the width w, the height h, and the penetration p) were developed with the aid of Minitab 19 software. The analysis of variance (ANOVA) for the models was conducted with a confidence level of 95% and a significant level of 5%.

3.1.1 The developed model of w

The prediction model of w is expressed by equation (22), and the ANOVA for the model of w is presented in Table 4. It is shown that the model and all the model terms $\{V_s, P_l,$ and $f_p\}$ are significant with the P-value inferior to 0.05. Among the process variables, the laser power P_l shows the highest contribution of 71.83%, followed by the scanning speed V_s and the powder feed rate f_p with a contribution of 23.85% and 2.20%, respectively. The determination coefficients of the model $\{R\text{-sq} = 97.89\%,\ R\text{-sq (adj)} = 96.62\%,\ R\text{-sq(pred)} = 92.72\%\}$ indicate a high prediction accuracy of the model. Therefore, the developed model of w can be utilized to predict the width of single tracks in the entire space of design with a high reliability level and it can be used as an objective function for the optimization problem.

$$\begin{aligned} w = {} & 1.3424 - 0.02992 * V_s + 0.002077 * P_l \\ & - 0.00303 * f_p(\text{mm}). \end{aligned} \tag{22}$$

3.1.2 The developed model of h

The prediction model of h is described by equation (23), and the ANOVA results for this model is given in Table 5. It is indicated that the model and all the model terms

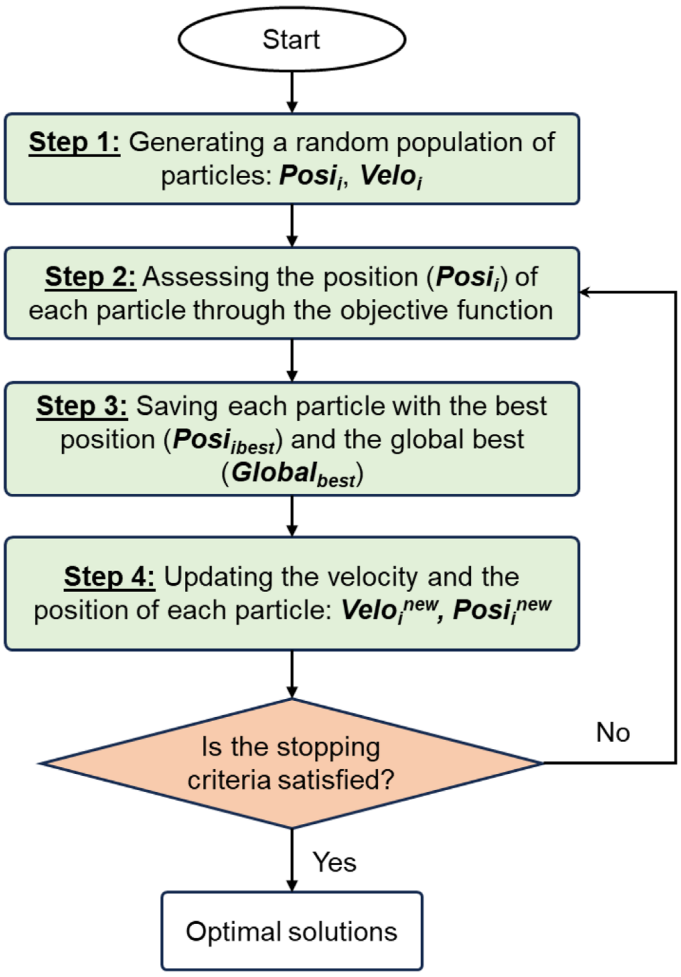

Fig. 3. Flowchart of PSO algorithm.

Table 4. ANOVA for w.

Source	DF	Seq SS	Contribution	Adj SS	Adj MS	F-value	P-value
Regression	3	0.088149	97.89%	0.088149	0.029383	77.15	0.000
V_s (mm/s)	1	0.021480	23.85%	0.021480	0.021480	56.40	0.001
P_l (W)	1	0.064688	71.83%	0.064688	0.064688	169.84	0.000
f_p (g/min)	1	0.001980	2.20%	0.001980	0.001980	5.20	0.072
Error	5	0.001904	2.11%	0.001904	0.000381		
Total	8	0.090053	100.00%				

R-sq = 97.89%, R-sq (adj) = 96.62%, R-sq (pred) = 92.72%.

Table 5. ANOVA for h.

Source	DF	Seq SS	Contribution	Adj SS	Adj MS	F-Value	P-Value
Regression	3	0.020772	97.08%	0.020772	0.006924	55.45	0.000
V_s (mm/s)	1	0.010668	49.86%	0.010668	0.010668	85.43	0.000
P_l (W)	1	0.006600	30.85%	0.006600	0.006600	52.85	0.001
f_p (g/min)	1	0.003504	16.38%	0.003504	0.003504	28.06	0.003
Error	5	0.000624	2.92%	0.000624	0.000125		
Total	8	0.021397	100.00%				

R-sq = 97.08%, R-sq (adj) = 95.33%, R-sq(pred) = 90.85%.

Table 6. ANOVA for p.

Source	DF	Seq SS	Contribution	Adj SS	Adj MS	F-value	P-value
Regression	3	0.005902	99.11%	0.005902	0.001967	185.40	0.000
V_s (mm/s)	1	0.000280	4.70%	0.000280	0.000280	26.40	0.004
P_l (W)	1	0.005222	87.68%	0.005222	0.005222	492.08	0.000
f_p (g/min)	1	0.000400	6.72%	0.000400	0.000400	37.71	0.002
Error	5	0.000053	0.89%	0.000053	0.000011		
Total	8	0.005955	100.00%				

R-sq = 99.11%, R-sq (adj) = 98.57%, R-sq(pred) = 97.40%.

{V_s, P_l, and f_p} show the P-value inferior to 0.05. Thus, they are significant model terms. In this model, the scanning speed V_s features the highest contribution of 49.86%, whereas the laser power P_l and the powder feed rate f_p show a smaller contribution of 30.85% and 16.38%, respectively. The determination coefficients of the model {R-sq = 97.08%, R-sq (adj) = 95.33%, R-sq(pred) = 90.85%} demonstrate that the model has a high prediction accuracy level. As a result, this model can predict the height of single tracks in the entire space of design with a high reliability level, and it can be used as an objective function for the optimization problem.

$$h = 0.0876 - 0.02108 * V_s + 0.000663 * P_l + 0.004028 * f_p(\text{mm}). \quad (23)$$

3.1.3 The developed model of p

The prediction model of w is expressed by equation (24), and the ANOVA for the model of p is presented in Table 6. It is revealed that the model and all the model terms {V_s, P_l, and f_p} are significant with the P-value inferior to 0.05. Among the process variables, the laser power P_l shows the highest contribution of 87.68%, followed by the powder feed rate f_p and the travel speed V_s with a contribution of 6.72% and 4.70%, respectively. The determination coefficients of the model {R-sq = 99.11%, R-sq (adj) = 98.57%, R-sq (pred) = 97.40%} confirm that the developed model of p exhibits a high prediction accuracy. Thereby, this model can be employed to predict the penetration of single tracks in the entire design space, and it can be used for the optimization problem.

$$p = -0.01672 - 0.003417 * V_s + 0.000590 * P_l - 0.001361 * f_p(\text{mm}). \quad (24)$$

3.2 Parametric influence analysis

Figure 4a shows the main effects of the process parameters on the width of single deposited tracks (w). It is shown that w decreases with an increment in the scanning speed V_s. A decreasing trend in w is also observed but with a lower rate when the powder feed rate f_p increases. On the other hand, w increases with an increase in the laser power P_l. Figure 5a shows the interactional effects of P_l, V_s, and f_p on w. It is also revealed that w increases with the increase in P_l with all values of V_s and f_p in the design space. w shows a decreasing trend with the increment in V_s for all values of P_l, while the interaction effects of (f_g and V_s) and (f_g and P_l) on w do not present uniform trends. This observation is in line with the ANOVA results presented in Table 4, where it is indicated that the laser power P_l shows the highest contribution of 71.83%, followed by the scanning speed V_s with a contribution of 23.85%, while the contribution of f_p is only of 2.20%. The effect trend of P_l and V_s on w observed in this study agrees with the those presented in [18,37]. In the current study and the previous studies [14,18], the w also an increasing trend with an increase in f_p. On the other hand, in the study of Sreekanth et al. [37] on the laser-DED of Inconel 718, the authors found that w features a decreasing trend with an increase in f_p. Such a difference could be explained by the insignificant contribution (only 2.20%) of f_p in the developed model of w. Theoretically, an increase in V_s leads to decreasing the interaction time of metal powder with the melting pool, resulting in a reduction of the tacking width and the deposited track width w. On the other hand, an increase in P can fuse more powder particles and enlarge the melting pool. Thus, the width track w increases.

Figure 4b shows the direct influence of P_l, V_s, and f_p on h, while Figure 5b exhibits the interaction effects of these parameters on h. It can be seen that h decreases as V_s increases from 6 mm/s to 10 mm/s while h increases as P_l increases from 200 W to 300 W. Similarly, h exhibits an increasing trend when f_p increases from 6 g/min to 18 g/min. These variation trends of h with the process parameter (V_s, P_l, and f_p) variation are also consistent with those observed in previous studies [19,32,38,39]. Due to V_s features the highest contribution of 49.86% to the h model (Tab. 5), V_s shows negative effects on h (i.e., h decreases when V_s increases) for all values of P_l and f_p. On the other hand, the interaction effects of (f_g and V_s) and (f_g and P_l) are not clear. This observation agrees with the ANOVA results given in Table 5, because f_g shows a small contribution to the h model (with a contribution of 16.38%). The deposited track height h decreases with an increase in V_s can be explained by the reduction of the powder amount per unit length along the deposition direction when V_s increases [14,40]. Meanwhile, h increases with an increment in the laser powder P_l. This is because when P_l increases the energy input increases and the amount of melted powder increases too, resulting in forming a great molting pool. As a result, both the w and h of the deposited track increase.

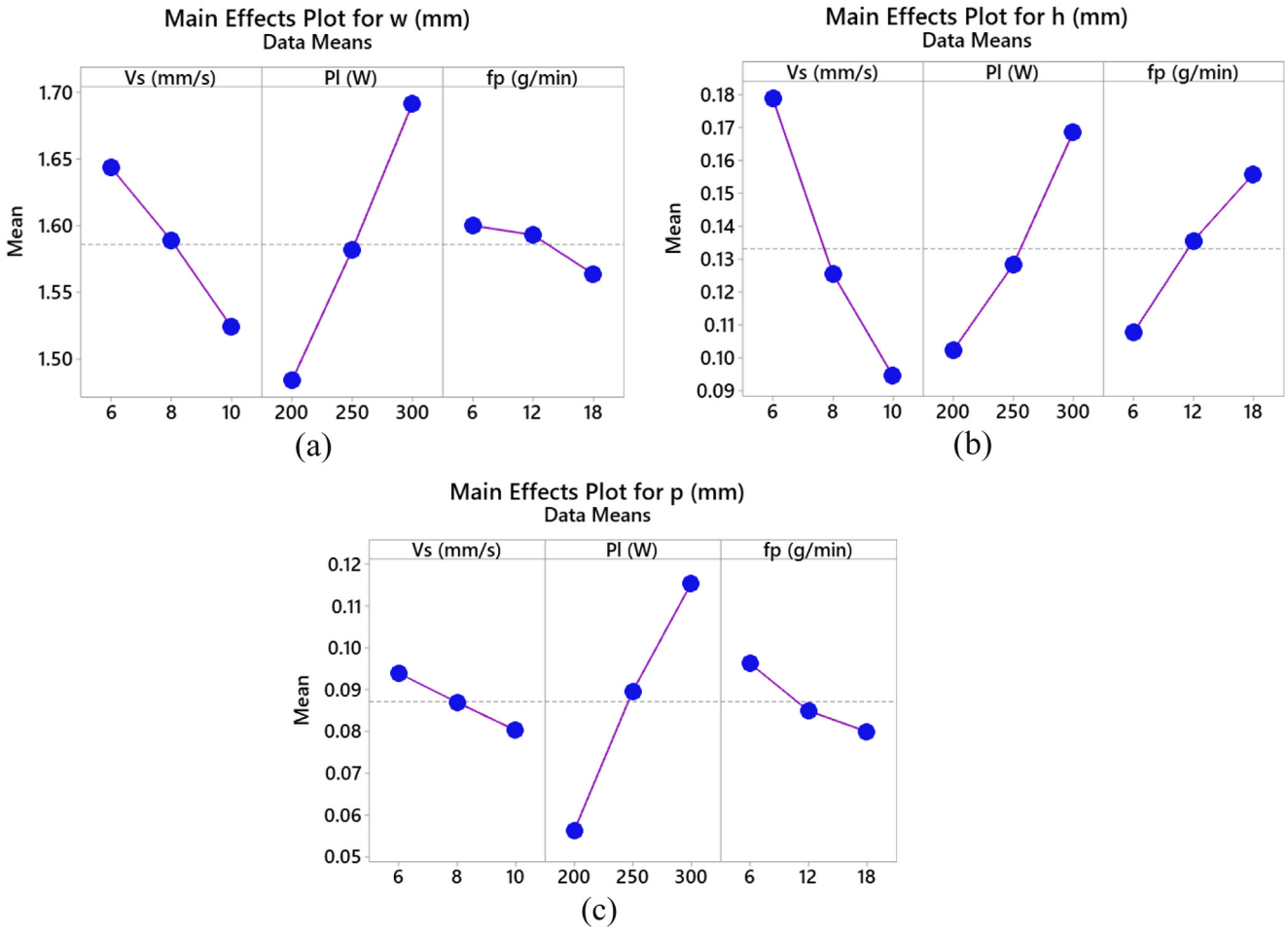

Fig. 4. Direct influences of parameters on (a) w, (b) h, and (c) p.

Figures 4c and 5c present the direct effects and the interactive effects of process variables on the penetration deep p of the deposited track, respectively. It can be observed that p increases for an increment in P_l (from 200 W to 300 W), while it is decreased with an augment in V_s (from 6 mm/s to 10 mm/s) and f_p (from 6 g/min to 18 g/min). In this case, due to the highest contribution to the p model of P_l (with 87.68% of contribution), the effect trend of P_l on p is the strongest. p increments with an increase in P_l for all values of V_s and f_p in the whole design space. On the other hand, with a small contribution value of f_p and V_s to the p model (6.72% and 4.70%, respectively), the effect trend of these variables on p is not uniform. The similar observation on the effects of P_l, V_s and f_p on p was reported in previous publications [14,32,38,40,41]. As explained in previous studies, when P_l increases, more laser energy input applied to the deposition process increases. As a result, p is deeper.

3.3 Optimization results

3.1.1 GRA results

Table 7 presents the results obtained by the GRA method. The normalized objectives were calculated by equations (1) and (2) for {w, p} and h, respectively. The grey-relational coefficients GRC were computed using equations (3)–(6), while the GRGs were achieved using equation (7). It is noted that the weight ω_j for each objective (i.e., w, p and h) was estimated from the experimental data by the CRITIC method, and the weight values were employed in both the GRA and TOPSIS methods. In this research, $\omega_w = \omega_p = 0.26$ and $\omega_h = 0.48$ Based on the GRGs' value, it is indicated that the run No. 7 with the highest value of GRG (0.703) is considered as the optimal solution. Hence, the optimal parameters estimated by the GRA methods are {$V_s = 10$ mm/s, $P_l = 200$ W, and $f_p = 18$ g/min} that produce a deposited track with {$w = 1.386$ mm, $h = 0.094$ mm, and $p = 0.042$ mm}.

3.3.2 TOPSIS results

Table 8 shows the results obtained by the TOPSIS method. The normalized data and the weighted normalized data were calculated by equations (8) and (9), respectively. The values of D_{BS_i} D_{WS_i} and C^i_{Index} ere calculated by equations (12)–(14), respectively. Based on the highest value of C^i_{Index} it is found that the process variables of the run No. 3 (i.e., $V_s = 6$ mm/s, $P_l = 300$ W, and $f_p = 18$ g/min) are considered as the optimal process variables, and they produced the deposited track with {$w = 1.745$ mm, $h = 0.235$ mm, and $p = 0.116$ mm}.

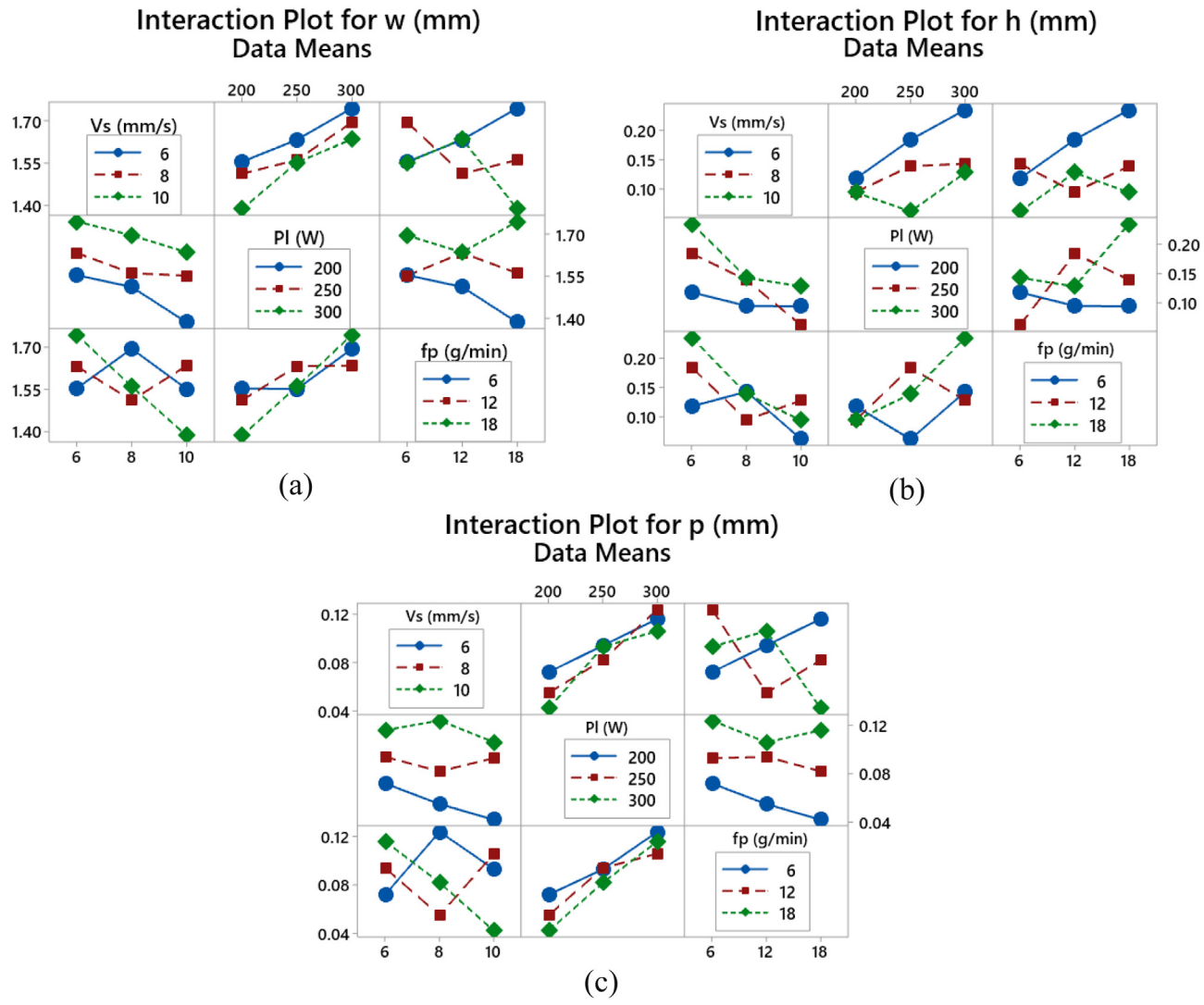

Fig. 5. Interaction influences of parameters on (a) w, (b) h, and (c) p.

Table 7. Optimization obtained by GRA.

No.	Normalized data			GRC			GRG	Rank
	w	h	p	w	h	p		
1	0.532	0.324	0.634	0.517	0.425	0.577	0.488	6
2	0.312	0.705	0.366	0.421	0.629	0.441	0.526	4
3	0.000	1.000	0.098	0.333	1.000	0.357	0.659	2
4	0.649	0.191	0.841	0.588	0.382	0.759	0.533	3
5	0.513	0.445	0.512	0.506	0.474	0.506	0.491	5
6	0.139	0.468	0.000	0.367	0.485	0.333	0.415	8
7	**1.000**	**0.185**	**1.000**	**1.000**	**0.380**	**1.000**	**0.703**	**1**
8	0.538	0.000	0.378	0.520	0.333	0.446	0.411	9
9	0.306	0.382	0.220	0.419	0.447	0.390	0.425	7

Table 8. Optimization obtained by TOPSIS.

No.	Normalized data			Weighted and normalized data			D_{BS_i}	D_{WS_i}	C^i_{Index}	Rank
	w	h	p	w	h	p				
1	0.264	0.162	0.232	0.085	0.133	0.069	0.135	0.081	0.374	5
2	0.319	0.322	0.273	0.089	0.208	0.090	0.077	0.141	0.646	2
3	**0.355**	**0.432**	**0.308**	**0.095**	**0.265**	**0.111**	**0.073**	**0.195**	**0.727**	**1**
4	0.306	0.286	0.247	0.082	0.107	0.052	0.159	0.077	0.326	8
5	0.362	0.444	0.273	0.085	0.157	0.078	0.115	0.096	0.455	3
6	0.343	0.219	0.467	0.092	0.161	0.118	0.131	0.091	0.411	4
7	0.345	0.434	0.235	0.076	0.106	0.040	0.159	0.088	0.357	7
8	0.322	0.229	0.387	0.085	0.070	0.089	0.201	0.031	0.135	9
9	0.371	0.341	0.467	0.089	0.144	0.101	0.136	0.077	0.361	6

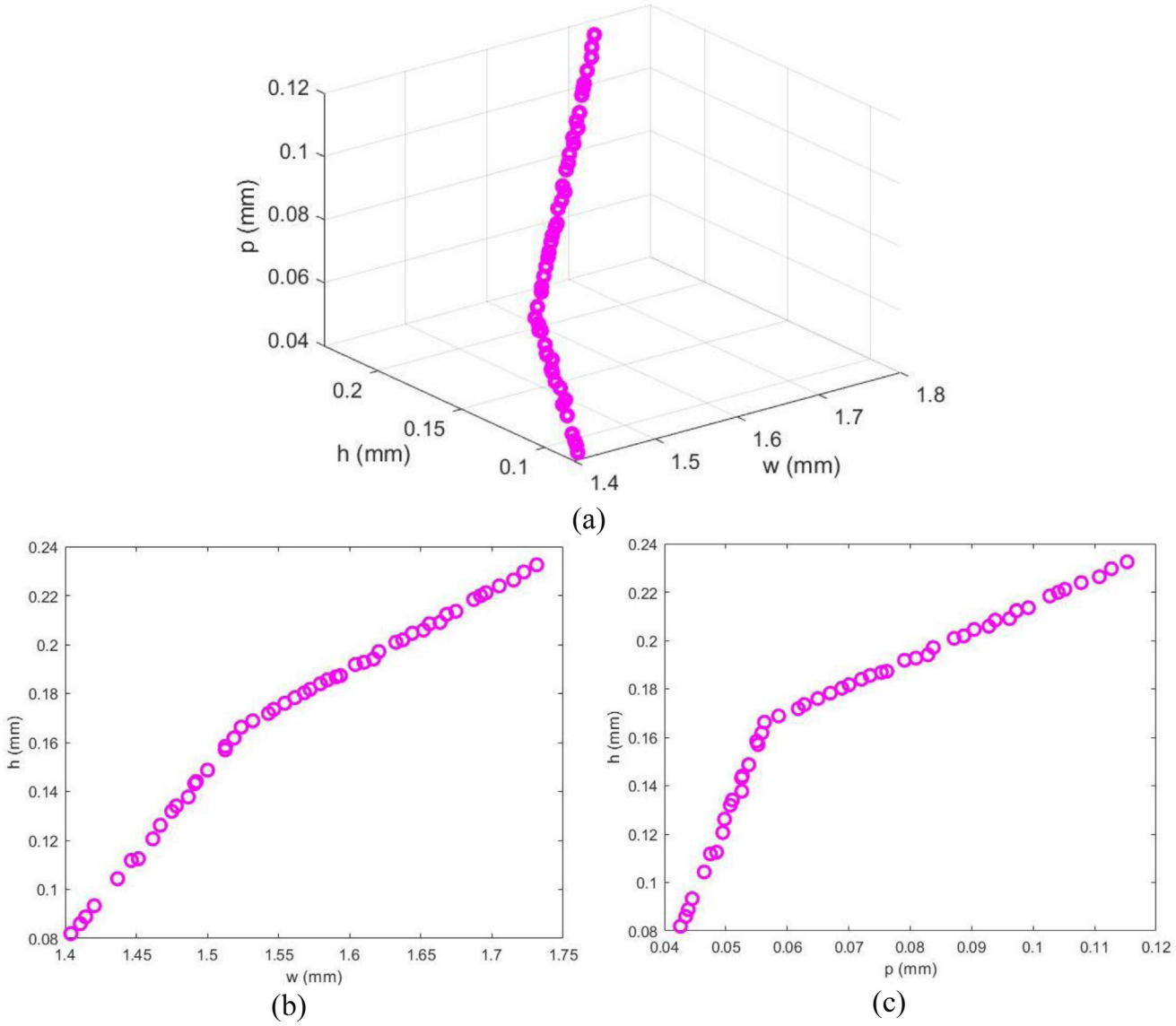

Fig. 6. PSO results: (a) Pareto of feasible optimal solutions, (b) w vs. h, and (c) p vs. h.

Table 9. Optimization obtained by TOPSIS from the PSO feasible optimal solutions.

No.	Feasible optimal solutions						D_{BS_i}	D_{WS_i}	C^i_{Index}	Rank
	V_s (mm/s)	P_l(W)	f_p (g/min)	w (mm)	h (mm)	p (mm)				
1	6.00	200.00	17.90	1.411	0.086	0.043	0.066	0.027	0.293	49
2	6.00	278.68	18.00	1.687	0.218	0.103	0.023	0.064	0.736	8
3	6.00	287.26	17.96	1.705	0.224	0.108	0.025	0.066	0.729	14
4	6.00	231.90	17.86	1.590	0.187	0.075	0.022	0.051	0.701	22
5	6.00	209.09	17.90	1.543	0.172	0.062	0.026	0.046	0.638	30
6	6.00	246.55	18.00	1.620	0.197	0.084	0.020	0.055	0.731	13
7	6.00	226.76	18.00	1.579	0.184	0.072	0.022	0.050	0.692	24
8	7.09	200.00	18.00	1.491	0.143	0.053	0.039	0.036	0.483	38
9	6.81	200.00	17.85	1.500	0.149	0.054	0.036	0.038	0.512	36
10	8.91	200.00	17.88	1.437	0.104	0.046	0.057	0.028	0.325	46
11	6.00	272.39	17.83	1.675	0.214	0.099	0.022	0.061	0.737	5
12	6.03	255.05	17.96	1.637	0.202	0.089	0.020	0.057	0.736	9
13	6.00	269.56	18.00	1.668	0.212	0.097	0.021	0.061	0.741	3
14	**6.00**	**263.63**	**18.00**	**1.656**	**0.208**	**0.094**	**0.021**	**0.059**	**0.742**	**1**
15	6.00	241.26	17.79	1.610	0.193	0.081	0.021	0.053	0.718	19
...	...	...	...	...	...	...	...	...	...	...
47	6.00	291.89	17.80	1.715	0.226	0.111	0.026	0.067	0.724	15
48	6.00	221.33	17.98	1.568	0.180	0.069	0.023	0.049	0.677	26
49	6.00	300.00	18.00	1.731	0.233	0.115	0.028	0.070	0.717	20
50	6.00	269.46	18.00	1.668	0.212	0.097	0.021	0.061	0.741	2

3.3.3 Results of PSO combined with TOPSIS

As mentioned earlier, the PSO algorithm generates a set of feasible optimal solutions. In this case, the prediction models of w, h, p (Eqs. (22), (23), and (24), respectively) were used as objective functions in PSO algorithms. The parameters of the PSO algorithm were chosen as follows: Both the population size and the repository size are equal to 50. The maximum generation number is 100. The inertia weight is 0.4. The individual confidence and swarm confidence factors are equal to 2. As a result, we obtained the Pareto of 50 feasible optimal solutions, as shown in Figure 6a. It can be found that it is difficult to select one feasible solution manually that satisfies the requirement (i.e., maximizing h while minimizing both w and p), because h increases with an increase in w and p (Figs. 6b and 6c). Therefore, the TOPSIS is utilized to select the most optimal solution among the feasible optimal solutions.

Table 9 shows the results of TOPSIS applied to the 50 feasible optimal solutions. It is shown that the solution No. 14 exhibits the highest value of C^i_{Index}. As a result, the most optimal solution selected by TOPSIS among the Pareto points is ($V_s = 6$ mm/s, $P_l = 263.63$ W, and $f_p = 18$ g/min), and they produced the deposited track with $\{w = 1.656$ mm, $h = 0.208$ mm, and $p = 0.094$ mm$\}$.

3.3.4 Comparison of different optimization results

Table 10 presents the comparison between different optimization results obtained with GRA, TOPSIS, and PSO combined with TOPSIS. Herein, the difference in results between the method A vs. the method B was defined by equation (25), where the $Atribute\,(A)$ *and* $Atribute\,(B)$s the values of the same attribute obtained by the method A and B, respectively.

$$The\ difference\ of\ A\ vs.\ B = 100\% * \frac{Atribute(A) - Atribute(B)}{Atribute(B)}. \quad (25)$$

It is indicated that the optimal solution obtained by TOPSIS shows the highest value of h, followed by the (PSO + TOPSIS) and GRA, respectively. The h obtained by TOPSIS is higher than that obtained by GRA up to 150%, while the optimal solution generated by (PSO +TOPSIS) shows a higher h value of 122% compared to that of GRA. Similarly, the values of w and p in TOPSIS and (PSO+TOPSIS) are higher than those obtained by GRA.

Compared to the TOPSIS method, the optimal parameters obtained by PSO+TOPSIS method enable producing the single track with the values of w, h, and p lower than those in TOPSIS with a reduction of 5%, 11% and 19%, respectively. As a result, in terms of w and p, the PSO+TOPSIS method provides better results, meanwhile, in terms of h, the TOPSIS is better. Indeed, h is related to the distance upwards the cladding nozzle moves prior to deposing the next layer or the layer height, while the penetration depth p is related to the bonding between the deposited layers through the dilution indicator,

Table 10. Comparison of optimization results obtained by GRA, TOPSIS and (PSO + TOPSIS).

Methods	V_s (mm/s)	P_l (W)	f_p (g/min)	w (mm)	h (mm)	p (mm)
GRA	10	200	18	1.386	0.094	0.042
TOPSIS	6	300	18	1.745	0.235	0.116
PSO+TOPSIS	6	264	18	1.656	0.208	0.094
Difference of TOPSIS vs. GRA (%)				26 (↑)	150 (↑)	176 (↑)
Difference of (PSO+TOPSIS) vs. GRA (%)				19 (↑)	122 (↑)	123 (↑)
Difference of (PSO+TOPSIS) vs. TOPSIS (%)				–5 (↓)	–11 (↓)	–19 (↓)

Fig. 7. Thin wall structures deposited with the optimal variables obtained in PSO + TOPSIS (i.e., $V_s = 6$ mm/s, $P_l = 264$ W, and $f_p = 18$ g/min).

$d = 100\% \times p/(p + h)$. Higher dilutions d lead to porosity and crack generation, which ultimately deteriorates the part's bond quality and mechanical performance [24,32,42]. In the current study, although the TOPSIS method provides a better objective h than the PSO+TOPSIS method (0.235 mm vs. 0.208 mm), it also provide a higher objective p (0.116 mm vs. 0.094 mm), leading to a higher dilution d (33% vs. 31%). Due to this reason, we consider that the PSO+TOPSIS method provides a better solution.

As a conclusion, in this research, compared to GRA and TOPSIS methods, PSO + TOPSIS offers the most appropriate objectives because it gives a solution balancing the objectives in the multi-objective optimization problem – i.e., maximizing h, while minimizing both (w and p).

Finally, the optimal process variables obtained by PSO + TOPSIS (i.e., $V_s = 6$ mm/s, $P_l = 264$ W, and $f_p = 18$ g/min) were used to build several thin-walled structures as shown in Figure 7. It can be seen that all the as-deposited components have good shape. There are also no major cracks appearing between the as-built part and the substrate, as well as between the deposited layers.

4 Conclusions

In this research, the influences of process variables (including the laser power P_l, the scanning speed of the deposition nozzle V_s, and the powder feeding rate f_p) on single deposited tracks' attributes in laser direct metal deposition (LDMD) of 316L stainless steel were explored and the optimum process variables for the deposition of 316L stainless steel thin-wall structures were identified, considering different multi-objective optimization problems. The main outcomes of this research can be summarized as follows:

– The laser powder P_l exhibits the highest impact contribution to the models of the deposited track width w and the deposited track penetration p with a contribution of 71.83% and 87.68%, respectively, among the process parameters (the scanning speed V_s, the laser power P_l, and the powder feed rate f_p). The scanning speed V_s exhibits the highest contribution to the models of the deposited track height h a contribution of 49.86%. Meanwhile, the powder feeding rate f_p shows an insignificant impact contribution to the w and p models.

- All the developed models of w, h, and p feature a high prediction accuracy with the values of determination coefficients R^2 of 97.89%, 97.08%, 99.11%, respectively, which demonstrate that they can be used to prediction w, h, and p with high confidence and precision levels.
- Moreover, the optimization results achieved by different methods (i.e., GRA, TOPSIS, and PSO+TOPSIS) demonstrated that the PSO combined with TOPSIS can be used to find out the most optimal process parameters (i.e., $V_s = 6$ mm/s, $P_l = 263.63$ W, and $f_p = 18$ g/min) to build thin-walled structures in SS316L by LDMD.
- The as-deposited part built with the optimal process variables shows smooth surfaces and a regular height, and without major cracks, validating their consistency.

Because of a significant role of the single tracks in the LDMD process, this research contributed an insight into the effects of the main process parameters (i.e., the scanning speed V_s, the laser power P_l, and the powder feed rate f_p) on the single tracks and the methods determining the optimal process parameters in LDMD of SS316L, to the academic community and specific applications. However, to provide a comprehensive understanding on the impact of the process parameters on the single tracks, other variables such as the laser beam spot diameter, the pressure and flowrate of carrying/shielding gas, the stand-off distance, and the particle size, need to be considered in the future work. The process optimization could also consider other outputs of the single tracks such as surface roughness, wetting angle, porosity, microhardness, etc.

Funding

This research is funded by Vietnam National Foundation for Science and Technology Development under grant number KC4.0-15/19-25.

Conflicts of interest

The authors have no competing interests to declare that are relevant to the content of this article.

Data availability statement

All data generated and analyzed during this study are included in this article.

Author contribution statement

T.K. Doan and V.T. Le are involved in the conceptualization and methodology; T.K. Doan, V.T. Le, and V. N. Duong contributed to the formal analysis and investigation; T.K. Doan and V.T. Le contributed to writing—original draft preparation; all the authors contributed to writing, review, and editing; T.K. Doan acquired the funding.

References

1. H.-S. Yoon, J.-Y. Lee, H.-S. Kim, M.-S. Kim, E.-S. Kim, Y.-J. Shin, W.-S. Chu, S.-H. Ahn, A comparison of energy consumption in bulk forming, subtractive, and additive processes: review and case study, Int. J. Precision Eng. Manufactur. Green Technol. **1** (2014) 261–279
2. N. Shamsaei, A. Yadollahi, L. Bian, S.M. Thompson, An overview of direct laser deposition for additive manufacturing; Part II: Mechanical behavior, process parameter optimization and control, Additive Manufactur. **8** (2015) 12–35
3. S.M. Thompson, L. Bian, N. Shamsaei, A. Yadollahi, An overview of direct laser deposition for additive manufacturing; Part I: Transport phenomena, modeling and diagnostics, Additive Manufactur. **8** (2015) 36–62
4. D.-G. Ahn, Directed energy deposition (DED) process: state of the art, Int. J. Precision Eng. Manufactur. Green Technol. **8** (2021) 703–742
5. T.D. Khoa, V.T. Le, V.N. Duong, V.C. Tran, Effects of scanning methods on cracking, microstructures and microhardness of Inconel 625 parts formed by direct laser metal deposition, Manufactur. Rev. **11** (2024) 2
6. W.E. Frazier, Metal additive manufacturing: a review, J. Mater. Eng. Perform. **23** (2014) 1917–1928
7. N. Guo, M. Leu, Additive manufacturing: technology, applications and research needs, Front. Mech. Eng. **8** (2013) 215–243
8. A. Carrozza, F. Mazzucato, A. Aversa, M. Lombardi, F. Bondioli, S. Biamino, A. Valente, P. Fino, Single scans of Ti-6Al-4V by directed energy deposition: a cost and time effective methodology to assess the proper process window, Metals Mater. Int. **27** (2021) 3590–3602
9. P.Y. Lin, F.C. Shen, K.T. Wu, S.J. Hwang, H.H. Lee, Process optimization for directed energy deposition of SS316L components, Int. J. Adv. Manufactur. Technol. **111** (2020) 1387–1400
10. A. Gonnabattula, R.S. Thanumoorthy, S. Bontha, A.S.S. Balan, V.A. Kumar, A.K. Kanjarla, Process parameter optimization for laser directed energy deposition (LDED) of Ti6Al4V using single-track experiments with small laser spot size, Opt. Laser Technol. **175** (2024) 110861
11. H. Javidrad, H. Aydin, B. Karakas, S. Alptekin, A.S. Kahraman, B. Koc, Process parameter optimization for laser powder directed energy deposition of Inconel 738LC, Optics Laser Technol. 176 (2024). https://doi.org/10.1016/j.optlastec.2024.110940
12. B. Han, R. Li, Q. Pi, Y. Shi, H. Qi, G. Sun, K. Bi, Deposit characteristics, morphology and microstructure regulation of single-track nickel-based alloy using quasi-continuous-wave laser direct energy deposition, Surf. Coat. Technol. **478** (2024) 130481
13. B. Zhang, H. Xiao, W. Zhang, H. Yang, Y. Wang, D. Peng, H. Zhu, B. Chen, Influence of the thermal conductivity of different CuCr0.8 substrate state on the formability of laser directed energy deposition Inconel718 single track, Mater. Character. **202** (2023) 113015
14. M. Dalaee, E. Cerrutti, I. Dey, C. Leinenbach, K. Wegener, Parameters development for optimum deposition rate in laser DMD of stainless steel EN X3CrNiMo13-4, Lasers Manufactur. Mater. Process. **9** (2022) 1–17
15. M. Biyikli, T. Karagoz, M. Calli, T. Muslim, A.A. Ozalp, A. Bayram, Single track geometry prediction of laser metal deposited 316L-Si via multi-physics modelling and regression analysis with experimental validation, Metals Mater. Int. **29** (2023) 807–820
16. G. Piscopo, E. Atzeni, S. Biamino, L. Iuliano, F. Mazzucato, A. Saboori, A. Salmi, A. Valente, Analysis of single tracks of IN718 produced by laser powder directed energy deposition process, Proc. CIRP **112** (2022) 340–345

17. M. Ansari, A. Mohamadizadeh, Y. Huang, V. Paserin, E. Toyserkani, Laser directed energy deposition of water-atomized iron powder: pProcess optimization and microstructure of single-tracks, Optics Laser Technol. **112** (2019) 485–493
18. M. Erfanmanesh, H. Abdollah-Pour, H. Mohammadian-Semnani, R. Shoja-Razavi, An empirical-statistical model for laser cladding of WC-12Co powder on AISI 321 stainless steel, Optics Laser Technol. **97** (2017) 180–186
19. H. El Cheikh, B. Courant, S. Branchu, J.Y. Hascoët, R. Guillén, Analysis and prediction of single laser tracks geometrical characteristics in coaxial laser cladding process, Opt. Lasers Eng. **50** (2012) 413–422
20. V. Errico, S.L. Campanelli, A. Angelastro, M. Mazzarisi, G. Casalino, On the feasibility of AISI 304 stainless steel laser welding with metal powder, J. Manufactur. Process. **56** (2020) 96–105
21. A. Ascari, A.H.A. Lutey, E. Liverani, A. Fortunato, Laser directed energy deposition of bulk 316L stainless steel, Lasers Manufactur. Mater. Process. **7** (2020) 426–448
22. S.L. Campanelli, A. Angelastro, C.G. Signorile, G. Casalino, Investigation on direct laser powder deposition of 18 Ni (300) marage steel using mathematical model and experimental characterisation, Int. J. Adv. Manufactur. Technol. **89** (2017) 885–895
23. A. Zardoshtian, M. Ansari, R. Esmaeilzadeh, A. Keshavarz-kermani, H. Jahed, E. Toyserkani, Laser-directed energy deposition of CuCrZr alloy: from statistical process parameter optimization to microstructural analysis, Int. J. Adv. Manufactur. Technol. **126** (2023) 4407–4418
24. S. Pandey, R. Srivastava, R. Narain, A.R. Vinod, Optimization of process parameters for direct energy deposition of 15Cr5Ni precipitation hardened stainless steel for aircraft parts repair and maintenance, Proc. Inst. Mech. Eng. C **236** (2022) 11505–11520
25. S. Chihaoui, I. Meddour, M. Athmane Yallese, S. Belhadi, K. Safi, Comparative assessment between DFA, NSGA-II coupled with TOPSIS, GRA, and TOPSIS for multiobjective optimization of gray cast iron turning process using CBN insert, Proc. Inst. Mech. Eng. E (2023). https://doi.org/10.1177/09544089231194039
26. V.T. Le, L. Hoang, M.F. Ghazali, V.T. Le, M.T. Do, T.T. Nguyen,
T.S. Vu, Optimization and comparison of machining characteristics of SKD61 steel in powder-mixed EDM process by TOPSIS and desirability approach, Int. J. Adv. Manufactur. Technol. **130** (2024) 403–424
27. T.T. Nguyen, L.H. Cao, T.A. Nguyen, X.P. Dang, Multi-response optimization of the roller burnishing process in terms of energy consumption and product quality, J. Cleaner Product. **245** (2020) 119328
28. Y. Huang, M.B. Khamesee, E. Toyserkani, A new physics-based model for laser directed energy deposition (powder-fed additive manufacturing): From single-track to multi-track and multi-layer, Opt. Laser Technol. **109** (2019) 584–599
29. K. Benarji, Y.R. Kumar, C.P. Paul, A.N. Jinoop, K.S. Bindra, Parametric investigation and characterization on SS316 built by laser-assisted directed energy deposition, Proc. Inst. Mech. Eng. L **234** (2020) 452–466
30. Z. Jardon, J. Ertveldt, M. Hinderdael, P. Guillaume, Process parameter study for enhancement of directed energy deposition powder efficiency based on single-track geometry evaluation, J. Laser Appl. 33 (2021). https://doi.org/10.2351/7.0000516
31. M. Poggi, A. Salmi, E. Atzeni, L. Iuliano, Effect of process parameters on AISI 316L single tracks by laser powder directed energy deposition, Proc. CIRP **118** (2023) 735–740
32. M. Ilanlou, R. Shoja Razavi, S. Haghighat, A. Nourollahi, Multi-track laser metal deposition of Stellite6 on martensitic stainless steel: Geometry optimization and defects suppression, J. Manufactur. Process. **86** (2023) 177–186
33. V.T. Le, Q.T. Doan, D.S. Mai, M.C. Bui, H.S. Tran, Van X. Tran, V.A. Nguyen, Prediction and optimization of processing parameters in wire and arc-based additively manufacturing of 316L stainless steel, J. Braz. Soc. Mech. Sci. Eng. **44** (2022) 394
34. V.T. Le, H. Paris, G. Mandil, D. Brissaud, A direct material reuse approach based on additive and subtractive manufacturing technologies for manufacture of parts from existing components, Proc. CIRP **61** (2017) 229–234
35. C.V. Nguyen, D.T. Nguyen, T.V. Le, Optimization of sustainable milling of SKD11 steel under minimum quantity lubrication, Proc. Inst. Mech. Eng. E **237** (2023) 907–916
36. V.T. Le, D.S. Mai, V.T. Dang, D.M. Dinh, T.H. Cao, V.A. Nguyen, Optimization of weld parameters in wire and arc-based directed energy deposition of high strength low alloy steels, Adv. Technol. Innovat. **8** (2023) 01–11
37. S. Sreekanth, K. Hurtig, S. Joshi, J. Andersson, Influence of laser-directed energy deposition process parameters and thermal post-treatments on Nb-rich secondary phases in single-track Alloy 718 specimens, J. Laser Appl. **33** (2021) 022024
38. P. Shayanfar, H. Daneshmanesh, K. Janghorban, Parameters optimization for laser cladding of Inconel 625 on ASTM A592 steel, J. Mater. Res. Technol. **9** (2020) 8258–8265
39. D.J. Corbin, A.R. Nassar, E.W. Reutzel, A.M. Beese, N.A. Kistler, Effect of directed energy deposition processing parameters on laser deposited Inconel ® 718: External morphology, J. Laser Appl. **29** (2017) 022001
40. M. Manjaiah, J.Y. Hascoët , M. Rauch, Effect of process parameters on track geometry, microstructural evolution on 316L stainless steel multi-layer clads, Mater. Sci. Eng. B **259** (2020) 114583
41. M. Ansari, A. Martinez-Marchese, Y. Huang, E. Toyserkani, A mathematical model of laser directed energy deposition for process mapping and geometry prediction of Ti-5553 single-tracks, Materialia **12** (2020) 100710
42. S. Kersten, M. Praniewicz, O. Elsayed, T. Kurfess, C. Saldana, Parametric study and multi-criteria optimization in laser directed energy deposition of 316l stainless steel, in ASME 2020 15th International Manufacturing Science and Engineering Conference, MSEC 2020. **1** (2020) 1–9

Cite this article as: Khoa Doan Tat , Van Thao Le, Nguy Duong Van , Prediction models and multi-objective optimization of the single deposited tracks in laser direct metal deposition of 316L stainless steel, Manufacturing Rev. **11**, 14 (2024)